Sub-shot-noise sensitivity in a ring laser gyroscope

Angela D. V. Di Virgilio[1], Francesco Bajardi[2,3], Andrea Basti[1,4], Nicolò Beverini[4], Giorgio Carelli[1,4], Donatella Ciampini[1,4], Giuseppe Di Somma[1,4], Francesco Fuso[1,4], Enrico Maccioni[1,4], Paolo Marsili[1,4], Antonello Ortolan[5], Alberto Porzio[2,6],* and David Vitali[7,8]
[1]*INFN Sez. di Pisa, Largo Bruno Pontecorvo 3, I-56127 Pisa, Italy*
[2]*INFN, Sez. di Napoli, Compl. Univ. Monte S. Angelo, Edificio G, Via Cinthia, I-80126, Napoli, Italy*
[3]*Scuola Superiore Meridionale, Largo San Marcellino 10, I-80138, Napoli, Italy*
[4]*Dipartimento di Fisica, Università di Pisa, Largo Bruno Pontecorvo 3, I-56127 Pisa, Italy*
[5]*INFN - LNL , Viale dell'Universit'a 2, 35020 Legnaro (PD), Italy*
[6]*Department of Civil and Mechanical Engineering – DICEM, Universitá di Cassino e Lazio Meridionale, 03043, Cassino, Italy*
[7]*Physics Division, School of Science and Technology, Università di Camerino Via Madonna delle Carceri 9, I-62032 Camerino (MC), Italy and*
[8]*INFN Sez. di Perugia, Via A. Pascoli, 06123 Perugia, Italy*
(Dated: January 5, 2023)

Absolute angular rotation rate measurements with sensitivity better than prad/sec would be beneficial for fundamental science investigations. On this regard, large frame Earth based ring laser gyroscopes are top instrumentation as far as bandwidth, long term operation and sensitivity are concerned. Their classical sensitivity limit is given by the shot–noise of the two beams counter propagating inside the cavity usually considered as two independent propagating modes. Thus, it is given by the sum of the shot–noise associated to each beam. Here we prove that the GINGERINO active ring laser prototype upper limiting noise allows an unprecedented sensitivity close to 10^{-15} rad/sec. This is more than a factor 10 better than the theoretical prediction so far accounted for ring lasers shot–noise.

Introduction – Light based interferometers have reached an extremely high level of sensitivity, reliability, and robustness. In most common interferometers, two separate beams, possibly coming from the same source, are injected in two separate paths and recombined to interfere so that differences in path-lengths even smaller than 10^{-14} times the wavelength can be resolved [1].

While such measurement scheme is possible thanks to the wave-nature of light, that shows-up as the interference of coherent beams, the corpuscular nature of light sets the intrinsic limit to the sensitivity attainable by interference. This limit is known as (photon) shot–noise and it is frequency independent. It intrinsically comes from the stochastic fluctuations in the photon number that, for coherent beams, are Poissonian distributed and so are the obtained photo-electrons [2].

Interferometer topology can be quite different. For example, it is possible to have paths defined by four mirrors located at the vertices of a square, thus defining a ring cavity where the two light beams circulates in clockwise and counter– clockwise directions. In this case, the two paths are equals, frequency jitters are negligible, and the interference of the two counter propagating beams carries information on the non reciprocal effects connected to the direction of circulation. If the frame supporting the four mirrors rotates, the two counter propagating beams complete the path at different times. In such a configuration, the interference measures the time derivative of the difference in phase acquired by the two beams, rather than the path spatial difference. This feature is the well known Sagnac effect, named after the French physicist George Sagnac [3, 4].

Sagnac interferometers, in particular the active versions also known as Ring Laser Gyroscopes (RLGs), are commonly used to measure inertial angular rotation. When connected to the Earth crust, they can be used to measure continuously the absolute angular rotation rate of the Earth. Thanks to their large bandwidth and high dynamic range, they can detect strong earthquakes and seismological signals in the frequency window $\sim 0.01 \div 30$ Hz, as well as tiny geodetic signals in the very low frequency domain ($< 10^{-3}$ Hz), showing an adequate sensitivity to probe General Relativity (GR) effects such as the Lense-Thirring and de Sitter [5].

Moreover, other non reciprocal effects related to propagation of the two light beams and connected to the space time structure or symmetries, can be investigated by RLGs, leading to results relevant in fundamental physics [6–8] when sensitivity of $5 \cdot 10^{-14}$rad/s or better are reached, corresponding to 1 part in 10^9 of the Earth rotation rate for Earth based apparata. At the same time, Sagnac interferometers are good candidates for investigating the interplay between GR and quantum systems and effects [9–13].

As any interferometer, sensitivity of Sagnac ones is limited by the photon shot–noise. Since the first model, elaborated in 1982 by Cresser et al. [14], following the concepts described in Ref. [15], it has been widely accepted that in Sagnac interferometers the two counter-propagating beams are independent. The corresponding shot–noise can be evaluated accordingly (see, e.g., [16, 17]): for example, in GINGERINO [18], a prototype

of the RLG array GINGER located inside the Gran Sasso National Laboratory of INFN, Italy, the model evaluates a shot–noise of about 18 prad/sec $\mathrm{Hz}^{-1/2}$, taking into account that its square optical cavity has side length of 3.6 m, total losses are 120 ppm, and the output power is 10 nW. However, in RLGs the two beams are generated inside the rotating cavity, where the same volume of active medium emits toward the two opposite directions. Therefore, the laser equations for the two counterpropagating beam amplitudes are coupled to each other [19]. While classical amplitude equations are effective for calculating the time dependence of mean values, inherent fluctuations requires a quantum description of the field modes, i.e. classical amplitudes have to be replaced by quantum field operators. Once the equations are transferred into a quantum frame, coupling of the two different modes implies the setting of some mutual correlation that may affect the noise features of the device and possibly its fundamental shot–noise limit.

Beating the quantum limit in gyroscopes has attracted interest in recent years, owing to the appealing possibilities of further improving their sensitivity. For passive gyroscopes [20], in analogy with what has been proposed [21] and then realised in Michelson interferometers (see [22] and references therein), the use of externally injected quantum states has been considered in different configurations [23–26] and experimentally realised [27–29] for going beyond the standard quantum limit. Other authors have considered the coupling of the ring modes to two–level atoms for realising effective mode coupling and so generating quantum correlation that may induce quantum enhancement [30]. Very recently, an experimental work reported a sensitivity below the standard shot-noise for phase estimation in a gyroscope equipped with a liquid crystal light valve (LCLV) for direct frequency measurement [31].

Recently, we have found that the ultimate sensitivity of the GINGERINO prototype is not consistent with the shot–noise calculated by the above mentioned independent beams model [32, 33]. In that case the final sensitivity has been evaluated by subtracting from the data all the known signals by linear regression methods and correcting for the laser dynamics [34]. In this Letter we report further measurements giving a conclusive proof that the noise limit of the instrument is well below the conventionally predicted shot–noise. Here, the noise floor is estimated by subtracting data obtained from two equivalent beating optical signals at the two outputs of a single beam–splitter. By principle, so doing we trace-out all the possible rotational signals providing an upper limit for the unavoidable quantum noise source.

RLG senses the projection of the angular velocity vector $\vec{\Omega}$ on the area of the closed polygonal cavity. The orientation of this area in space is determined by the area versor $\vec{n}$. The relationship between the Sagnac pulse frequency ω_s and the angular rotation rate Ω reads

$$\omega_s = 8\pi \frac{A}{\lambda L} \Omega \cos\theta \,, \tag{1}$$

where A is the area of the cavity, L the perimeter, λ the wavelength of the light, and θ the angle between $\vec{n}$ and $\vec{\Omega}$.

So far, large RLGs have been dedicated to very low frequency measurements [35, 37] below 30 Hz, where physical and geophysical investigations are relevant. In this range, apart from those of scientific interest, there are signals of different nature such as, human activity, microseismicity of the crust generated by the ocean, tides and polar motion, temperature and pressure variations, that may reduce the instrument sensitivity. Despite that, available measurements show sensitivity ranging from the nrad/s to tens of prad/s [17, 32, 36]. It is convenient to express the sensitivity as angular rotation rate, and in order to avoid confusion, the angular frequency will be indicated as small cap ω and the corresponding angular velocity as capital Ω, the two quantities are connected by the geometrical scale factor of Eq. (1).

Data analysis and GINGERINO – GINGERINO has shown evidence of a limiting noise smaller than expected [33]. In order to gain useful insights into such unexpected result, we have improved the setup with the aim to obtain a direct estimation of the stochastic noise itself, hereafter denoted ω_{Tn}. In principle, $\Omega_{Tn} \geq \Omega_{sn}$, where Ω_{sn} indicates the shot–noise, being Ω_{Tn} the sum of various noise contributions. Contrarily to Ω_{sn}, Ω_{Tn} is not a flat noise and, for GINGERINO, it shows the limit of $2-3$ prad/s in 1 s measurement time. The corresponding Modified Allan Deviation reaches the value of 2.1 ± 0.01 frad/s in 2.5 days of integration time, that corresponds to $4.3 \cdot 10^{-11}$ the Earth rotation rate.

The two counter–propagating beams leaving the cavity of our RLG prototypes are combined at a beam–splitter placed at one of the cavity corners. The two resulting mixed beams, observed by two identical photodiodes, contain the measured beat note ω_m. Since in this general treatment an ideal behavior is assumed, neglecting any laser systematics, we will consider $\omega_m = \omega_s$ the signal of interest. Without loss of generality, it is possible to state that photodiode signals can be expressed as $S_i = A_g \cdot (-1)^i \cdot (\cos(\omega_s + \omega_n) \cdot t) + \phi_n) + V_{n_i}$, with $i = 1, 2$, where A_g is a gain factor, ω_n indicates the stochastic noise affecting the frequency itself, ϕ_n is the stochastic term of the phase, and V_{n_i} is any noise added outside the cavity [38]. The reconstructed frequency signal from each photodiode is defined by $\omega_i = \omega_s + \omega_{Tn_i}$, where ω_{Tn_i} takes into account all noise terms at once, since it is not possible to discriminate among different noise sources. Therefore, ω_{Tn_i} has to be considered an upper limit to ω_n. In this configuration, the two measurements are independent one another and each of them contains the frequency signal ω_s plus the sum of differ-

ent noise contributions: the noise of the two laser beams in the cavity, mainly of stochastic nature, and the noise picked up outside the cavity, containing disturbances induced by the environment and stochastic terms.

In order to have a better estimate of the limiting noise and of the signal, we consider the signal difference ($S = S_1 - S_2$) and define $\omega_d = \omega_s + \omega_{Tn_d}$ the corresponding frequency signal. It is straightforward to note that, considering the stochastic noise, ω_d has a signal to noise ratio $\sqrt{2}$ larger than the single photodiode measurements, because the Sagnac signal is doubled while the stochastic noise is increased by a $\sqrt{2}$ factor. Moreover, in ω_{Tn_d} disturbances produced outside the cavity, and common to both photodiodes, are cancelled out.

Let us consider ω_{n12}, defined as the difference $\omega_{n12} = \omega_1 - \omega_2$, that contains the quadratic sum of all stochastic terms of the two interference signals and the difference between the disturbances of environmental origin recorded by the two detectors, similarly to ω_{Tn_d}. We can consider ω_{n12} as an upper limit to the stochastic noise generated inside the cavity and simple manipulations lead to $\omega_{n12} \sim 2 \cdot \omega_{Tn_d}$. The factor 2 has been checked with simulated data. In summary, ω_d provides the best angular rotation rate estimation, while $\omega_{Tn_d} = \omega_{n12}/2$ measures its sensitivity noise limit.

At this point, it is necessary to take into account the data analysis procedure. The procedure adopted for frequency estimation is based on the Hilbert transform. We first recover the phase from the analytic signal and then evaluate the frequency ω by differentiation. In general, interferograms, and monobeams intensities, are acquired at 5 kSa/s. The subsequent analysis is performed with no down sampling. When the analysis is focused below 1 Hz, a digital band pass filter centered on the mean beating frequency and with a ± 12 Hz width is applied before the Hilbert transform [39]. The band–pass filter is not used for high frequency investigation.

It is worth noticing that performances of the frequency estimation procedure must be evaluated by simulation as it is based on a non linear transformation of data. Three main noise sources are identified: the white frequency noise ω_n, the white phase noise ϕ_n and a phase diffusion noise ϕ_W modeled as a Wiener process.

Figure 1 shows the response of the reconstruction procedure to the injection of these three types of noise. In particular, we report the Amplitude Spectral Distribution (ASD) of the injected noise ω_n (green) and of the corresponding reconstructed signal (purple), as well as the ASD of the reconstructed signal injecting ϕ_n, $\phi_n = \omega_n \cdot \bar{t}$ with $\bar{t} = 0.02$ s integration time (red), and ϕ_W (yellow).

The contribution of the white stochastic frequency noise ω_n is reconstructed by the analysis process as a frequency white noise a factor 20 higher in the low frequency range ($10^{-2} \div 20$ Hz), which grows linearly at higher frequencies. At frequencies above 20 Hz, its behaviour becomes indistinguishable from that reconstructed when

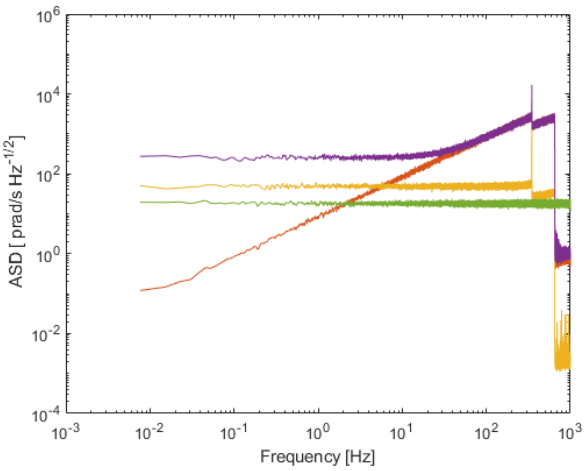

FIG. 1. ASD of the injected noise Ω_n (green) and of the corresponding reconstructed signal (purple); ASD of the reconstructed frequency obtained by injecting ϕ_n, with $\bar{t} = 0.02$ s integration time (red), and φ_W (yellow). The injected noise level is 20 prad/s Hz$^{-1/2}$.

the white phase noise ϕ_n is injected, that produces a power spectrum proportional to frequency over the full frequency span. On the other hand, the phase diffusion noise, simulated as a Wiener process, produces a constant ASD, a factor of 2 higher than the level of the injected noise. It's worth noticing that all ASD of the reconstructed signals show a discontinuity at the Sagnac frequency.

Experimental spectra of RLG prototypes - We have analysed experimental data produced by four distinct large frame RLG prototypes [40]. In Fig. 2 we report the ASD for G–Wettzell [17], GINGERINO, and GP2 [41] while the ASD of ROMY [35], that shows very similar behaviour, is not reported. Typically, the frequency range below 0.1 Hz is affected by laser systematics and contains signals of geophysical origin, for this reason it is not suitable for any noise investigation. The minimum of the ASD is in the frequency window $0.1 \div 1$ Hz, where microseismicity originated by the oceans is present. The region above 5 Hz contains regular signals but also a characteristic tail linearly growing with frequency.

Despite big differences, due to the different structure and location, all three ASD show the characteristic high frequency behavior linearly growing with frequency. This feature, being compatible with a flat phase noise, indicates that, at least in this range of frequencies, there is a stochastic noise floor dominated by a frequency independent phase noise.

Because of its noisy location, GP2 data show larger noise (approximately a factor of ten above the other prototypes). Moreover, different disturbances are affecting the cavity at low frequency, as the microseismicity from oceans, well visible in G. However, in the region around 1

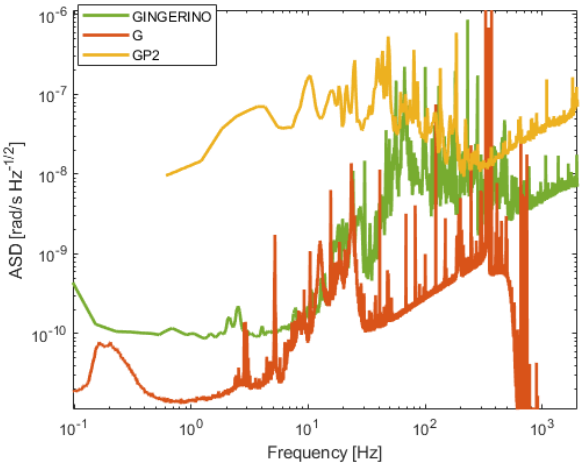

FIG. 2. ASD of the data, expressed as angular rotation rate, of G Wettzell, GINGERINO, and GP2. The high frequency part of the spectrum shows a very characteristic tail constantly rising with frequency. G, owing to its monolithic structure, is very quiet and 1 hour has been used for the ASD, while for GINGERINO 15 minutes of time have been selected. GP2 is 1.6 m in side, and it is located in a rather noisy environment, that explains the occurrence of a larger noise. Data from G are acquired at 2 kSa/s, the cut-off occurring around 0.5 kHz is due to the analysis procedure.

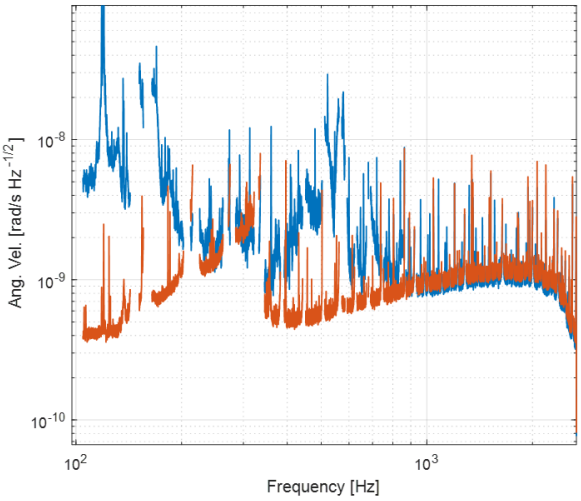

FIG. 3. ASD of $\Omega_{n12}/2$ (red) compared with Ω_d (blue) spectrum at high frequency. The noise floor agreement is good. Some peaks due to electronics or environmental origin have been removed.

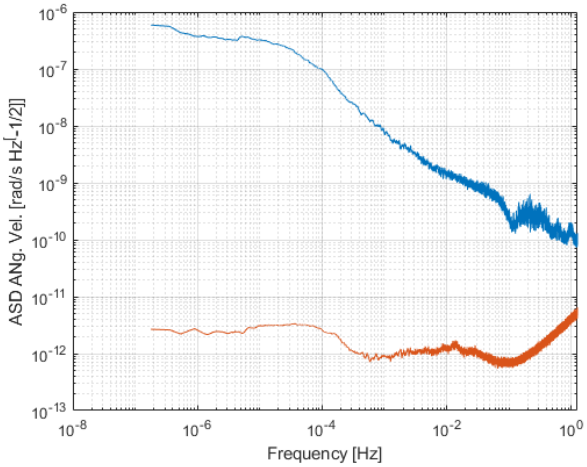

FIG. 4. ASD of Ω_{Tn} (red) compared with Ω_d (blue) spectrum at low frequency. In this spectrum two hours of data around the big Mw 5.9 event have been removed (see [42]); when included, the low frequency bump increases.

Hz, where the curves exhibit their minimum, amplitude is smaller than the one expected assuming $\Omega_n = 18$ prad/s in 1 s of measurement time, which would correspond to 0.4 nrad/s after the reconstruction.

Ω_{Tn} was evaluated using 20 days of GINGERINO data starting from October 29, 2022. The whole set of data have been acquired at 5 kSa/s. The high frequency part of the spectrum has been investigated using small portions of data, corresponding typically to 3 hours, and avoiding any filtering around the beat note (280.4 Hz). The low frequency part, from DC up to 5 Hz, has been analysed following the standard procedure of GINGERINO which evaluates the different terms: ω_m, ω_{s0}, ω_ξ, and ω_{ns}, the latter relating to null shift [42].

In the following we report the results using ω_{s0}, which is the best approximation of the Sagnac frequency, since it takes into account the back-scatter noise, avoiding the use of linear regression usually employed to subtract effects of electronic origin (ω_ξ), and null shift due to the laser dynamics (ω_{ns}). However, it has been checked that very similar results are obtained using the beat notes itself, ω_m, or estimating the true Sagnac signal ω_s by linear regression [33].

The ASD of reconstructed signals Ω_d and Ω_{n12} are shown in Fig. 3: noise floors at high frequency are in good agreement with each other.

Fig. 4 compares Ω_d and Ω_{Tn}, with the latter exhibiting above 0.1 Hz the characteristic phase noise behavior, and being almost flat at lower frequency, with a level around 2 prad/s $\mathrm{Hz}^{-1/2}$, a factor 10 below the expected shot–noise, and 200 times below the one obtained by taking into account the analysis procedure.

Fig. 5 reports the corresponding Overlapped and Modified Allan Deviations (obtained by STABLE32), demonstrating levels of 4 and 2.63 frad/s in approximately 2.4 days of integration time, respectively, corresponding to 1.23 and 1.87 in 10^{10} the Earth rotation rate, a level sufficient for detecting fundamental physics effects with an array of RLGs [7, 8].

Summary - It is proved that, below 0.1 Hz, the large RLG prototype GINGERINO shows a limiting noise floor

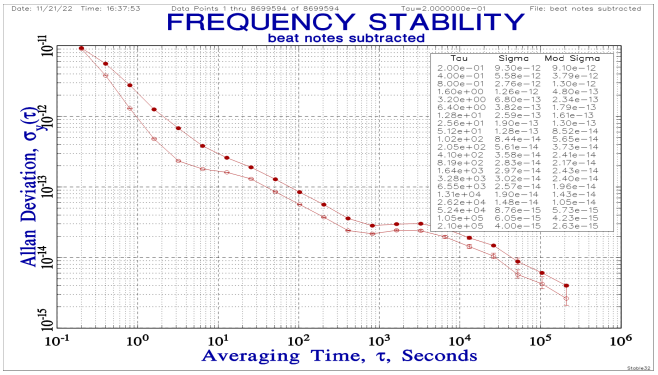

FIG. 5. Overlapped and Modified Allan Deviation of Ω_{Tn} expressed in rad/s. The plot have been obtained by using STABLE32 freely available at: http://www.stable32.com/

in the prad/s $\mathrm{Hz}^{-1/2}$ range, well below what expected for the shot–noise in this type of apparatus taking for granted the independent beam model [14]. This experimental noise limit has been obtained by subtracting two independent rotation signals. These signals come from the two outputs of a single beam–splitter placed at one of the cavity corners to let the counter propagating beams interfere. So doing, the estimated noise level represents an upper limit to the inherent quantum noise affecting the apparatus. While this experimental finding suggests that a complete quantum model of the system should take into account the complex interdependent dynamics of the counter–propagating beams, it gives a conclusive proof of the feasibility of fundamental physics measurements once an array of RLGs is available. In a forthcoming study we will develop a model that, tracing back from the detector scheme, accounts for all the possible interactions between the counter–propagating beams and the laser medium. A full quantum picture is required so to have a theoretical shot–noise estimation to be compared with the presented experimental finding.

ACKNOWLEDGEMENT

The authors thank K. U. Schreiber, J. Kodet, H. Igel and A. Brotzer for providing the data of G Wettzell and ROMY to investigate the high frequency noise.

* Corresponding author alberto.porzio@na.infn.it

[1] Abbott, B.P., *et al.*, Living Rev. Relativ. Living Rev. Relativ. **23**, 3 (2020).
[2] B. Picinbono, C. Bendjaballah, and J. Pouget, J. Mat. Phys. **11**, 2166 (1970).
[3] G. Sagnac, Comptes Rendus **157**, 708 (1913); **157**, 1410 (1913).
[4] The Sagnac effect: 100 years later / L'effet Sagnac : 100 ans après Special Issue edited by Gauguet Alexandre, Compte Rendus Physique, **15**, Issue 10, (2014).
[5] A. Tartaglia, A.D.V. Di Virgilio, J. Belfi, N. Beverini, and M.L. Ruggiero, Eur. Phys. J. Plus **132**, 73 (2017).
[6] M.O. Scully, M.S. Zubairy, and M.P. Haugan, Phys. Rev. A **24**, 2009 (1981).
[7] S. Capozziello, *et al.*, Eur. Phys. J Plus, **136**, 394 (2021).
[8] C. Altucci, *et al.* Mathematics and Mechanics of Complex Systems (MEMOCS), to be published arXiv:2209.09328 (2022).
[9] M. Fink, *et al.*, Nat. Commun. **8**, 1 (2017).
[10] S. Restuccia, M. Toroš, G. M. Gibson, H. Ulbricht, D. Faccio, and M. J. Padgett, Phys. Rev. Lett. **123**:110401 (2019).
[11] M. Toroš, S. Restuccia, G. M. Gibson, M. Cromb, H. Ulbricht, M. Padgett, and D. Faccio, Phys. Rev. A **101**, 043837 (2020).
[12] M. Toroš, M. Cromb, M. Paternostro, and D. Faccio, Phys. Rev. Lett. **129**:260401 (2022).
[13] M. Cromb, S. Restuccia, G. M. Gibson, M. Toroš, M. J. Padgett, and D. Faccio, arXiv: 2210.05628 (2022).
[14] J.D. Cresser, W.H. Louisell, P. Meystre, W. Schleich, and M.O. Scully, Phys. Rev. A **25**, 2214 (1982); J.D. Cresser, D. Hammonds, W.H. Louisell, P. Meystre, and H. Risken, Phys. Rev. A **25**, 2226 (1982); J.D. Cresser, Phys. Rev. A **26**, 398 (1982).
[15] T. Dorschner, H. Haus, M. Holz, I. Smith, and H. Statz, IEEE J. Quantum Electron. **16**, 1376 (1980).
[16] W.W. Chow, J. Gea-Banacloche, L.M. Pedrotti, V.E. Sanders, W. Schleich, and M.O. Scully, Rev. Mod. Phys. **57**, 61 (1985).
[17] K.U. Schreiber and K.U. Wells, Rev. Sci. Instrum. **84**, 041101 (2013).
[18] Jacopo Belfi, *et al.* Review of Scientific Instruments **88**, 034502 (2017);
[19] J.R. Wilkinson, Prog. Quant. Electr. **11**, 1 (1987).
[20] K. Liu, F. L. Zhang, Z. Y. Li, X. H. Feng, K. Li, Z. H. Lu, K. U. Schreiber, J. Luo, and J. Zhang, Opt. Lett., **44**, 11, 2732 (2019).
[21] C.M. Caves, Phys. Rev. D **23**,1693 (1981).
[22] J. Heinze, K. Danzmann, B. Willke, and H. Vahlbruch, Phys. Rev. Lett. **129**, 031101 (2022).
[23] A. Kolkiran and G.S. Agarwal, Opt. Expr. **15**, 6798 (2007).
[24] A. Luis, I. Morales, and A. Rivas, Phys. Rev. A **94**, 013830 (2016).
[25] M.R. Grace, C.N. Gagatsos, Q. Zhuang, and S. Guha, Phys. Rev. Applied **14**, 034065 (2020).
[26] L. Jiao and J.-H. An, Noisy quantum gyroscope, Photonic Research, to be published arXiv:2201.10934v1 (2022)
[27] M. Mehmet, T. Eberle, S. Steinlechner, H. Vahlbruch, and R. Schnabel, Opt. Lett. **35**, 1665 (2010).
[28] K. Liu, C. Cai, J. Li, L. Ma, H. Sun, and J. Gao, Appl. Phys. Lett. **113**, 261103 (2018).
[29] M. Fink, F. Steinlechner, J. Handsteiner, J.P. Dowling, T. Scheidl, and R. Ursin, New J. Phys. **21**, 053010 (2019).
[30] W. Cheng, Z. Wang, and X. Wang, Phys. Rev. A **105**, 023716 (2022).
[31] J.C. Howell, M. Kahn, E. Grynszpan, Z.R. Cohen, S. Residori, and U. Bortolozzo, Phys. Rev. Lett. **129**, 113901 (2022).

[32] A.D.V. Di Virgilio, *et al.*, Phys. Rev. Res. **2**, 032069(R) (2020).
[33] A.D.V. Di Virgilio, *et al.*, Eur. Phys. J. C **81**, 400 (2021).
[34] A.D.V. Di Virgilio, N. Beverini, G. Carelli, D. Ciampini, F. Fuso, and E. Maccioni, Eur. Phys. J. C **79**, 573 (2019); A.D.V. Di Virgilio, N. Beverini, G. Carelli, D. Ciampini, F. Fuso, U. Giacomelli, E. Maccioni, and A. Ortolan, Eur. Phys. J. C **80**, 163 (2020).
[35] H. Igel, *et al.*, Geophys. J. Int. **225**, 684-698 (2021).
[36] A. Gebauer, *et al.*, Phys. Rev. Lett. **125**, 033605 (2020).
[37] A.D.V. Di Virgilio, *et al.* Eur. Phys. J. C **82**, 824 (2022).
[38] The last term includes noise equivalent power of the photodiode, or amplitude fluctuation of the light at the detector, etc.
[39] Different filters can be adopted: in the present analysis we used a filter based on FFT.
[40] The considered prototypes, all but ROMY employing square optical cavities, are: (i) G of the geodetic observatory of Wettzell, Germany, located on the Earth surface inside a pressure tight bunker and featuring a monolithic structure in ZERODUR with 16 m perimeter and mirrors optically contacted to the central rigid structure; (ii) GINGERINO, located inside the very quiet environment of the Gran Sasso underground laboratory of INFN, Italy, consisting of a heterolytic (HL) structure done attaching together different rigid pieces in granite and mirrors contained inside stainless steel boxes, forming a 14.4 m perimeter cavity; (iii) ROMY, an array RLGs located in the geophysical observatory close to Munich, composed of 4 HL triangular RLGs with 36 m perimeter; (iv) GP2, with a 6.4 m perimeter and HL structure, located inside the basement of the INFN Pisa Section, Italy.
[41] E. Maccioni, N. Beverini, G. Carelli, G. Di Somma, A. Di Virgilio, and P. Marsili, Appl. Opt. **61**, 9256-9261 (2022).
[42] GINGERINO is free running, the temperature is stable at the level of fractions of a degree, accordingly the cavity perimeter changes causing a large number of mode jumps. In the considered period, for two times the interferometer has operated in split mode for several hours, approximately 50 minutes are missing, since it has been necessary to restart the data acquisition system. In this time window a large earthquake swarm about $200 - 300$ km apart is contained, for this reason 2 hours of data around the big shock with Mw 5.6 of November 9, 2022, have been removed. In summary the full data set is continuous with 4% of missing points.